The equation of state at finite temperature: Structure and composition of protoneutron stars

G F Burgio[1]∗, M Baldo[1], H Chen[2] and H-J Schulze[1]

[1] INFN Sezione di Catania, Via S. Sofia 64, 95123 Catania, Italy
[2] Department of Physics, China University of Geoscience, 430074 Wuhan, People's Republic of China

E-mail: baldo@ct.infn.it, burgio@ct.infn.it, huanchen.phy@gmail.com, schulze@ct.infn.it

Abstract. We study the hadron-quark phase transition at finite temperature in the interior of protoneutron stars, combining the equation of state obtained within the Brueckner-Hartree-Fock approach for hadronic matter with the MIT bag and the Dyson-Schwinger models for quark matter. We discuss the dependence of the results on different nuclear three-body forces and on details of the quark model. We find that a maximum mass exceeding two solar masses can be obtained with a strong three-body force and suitable parameter values in the Dyson-Schwinger model.

1. Introduction

It is generally believed that a neutron star (NS) is formed as a result of the gravitational collapse of a massive star ($M \gtrsim 8M_\odot$) in a type-II supernova [1, 2]. Just after the core bounce, a protoneutron star (PNS) is formed, a very hot and lepton-rich object, where neutrinos are temporarily trapped. The following evolution of the PNS is dominated by neutrino diffusion, which results first in deleptonization and subsequently in cooling. The star stabilizes at practically zero temperature, and no trapped neutrinos are left [3, 4]. The dynamical transformation of a PNS into a NS could be strongly influenced by a hadron-quark phase transition in the central region of the star [5, 6]. Calculations of PNS structure, based on a microscopic nucleonic equation of state (EOS), indicate that for the heaviest PNS, close to the maximum mass (about two solar masses), the central baryon density reaches values larger than $1/\mathrm{fm}^3$. In this density range the nucleon cores (dimension ≈ 0.5 fm) start to touch each other, and it is likely that quark degrees of freedom will play a role.

In previous articles [7, 8, 9] we have studied static properties of PNS using a finite-temperature hadronic EOS including also hyperons [10] derived within the Brueckner-Bethe-Goldstone (BBG) theory of nuclear matter. An eventual hadron-quark phase transition was modeled within an extended MIT bag model [11, 12, 13]. In the present work we consider a more sophisticated quark model, the Dyson-Schwinger model (DSM) [14, 15, 16, 17].

The study of hybrid stars is also important from another point of view: Purely nucleonic EOS are able to accommodate fairly large (P)NS maximum masses [18, 19, 20, 21, 22], but the appearance of hyperons in beta-stable matter could strongly reduce this value [22, 23, 24]. In this case the presence of non-baryonic, i.e., "quark" matter would be a possible manner to stiffen the EOS and reach large NS masses. Heavy NS thus would be hybrid quark stars.

∗Speaker

The paper is organized as follows. In section 2 we review the determination of the baryonic EOS in the BHF approach at finite temperature. Section 3 concerns the QM EOS according to the DSM, comparing also with the MIT bag model for reference. In sections 4 and 5 we present the results regarding (P)NS structure, combining the baryonic and QM EOS for beta-stable nuclear matter via a Gibbs phase transition construction. Section 6 contains our conclusions.

2. EOS of nuclear matter at finite temperature in the Brueckner approach

The starting point in the many-body theory of the finite-temperature EOS is the calculation of the grand-canonical potential Ω. In the Bloch – De Dominicis formalism [25] it is given by $\Omega = \Omega_0 + \Delta\Omega$, where

$$\Omega_0 = -\frac{2V}{\pi^2}\int_0^\infty k^2 dk \left[\frac{1}{\beta}\ln\left(1+e^{-\beta(e_k-\mu)}\right)+n(k)U(k)\right] \tag{1}$$

is the grand-canonical potential for independent particles with Hamiltonian

$$H_0 = \sum_k \left(\frac{k^2}{2m}+U(k)\right)a_k^\dagger a_k\,, \tag{2}$$

μ is the chemical potential and U is the single-particle potential. The interaction part $\Delta\Omega$ of the grand-canonical potential is given by

$$\Delta\Omega = \frac{e^{2\beta\mu}}{2}\int_{-\infty}^{\infty}\frac{d\omega}{2\pi}e^{-\beta\omega}\,\mathrm{Tr}_2\left[\arctan\left(\pi\mathscr{K}(\omega)\delta\left(H_0-\omega\right)\right)\right]. \tag{3}$$

The trace in the previous equation is taken in the space of anti-symmetrized two-body states and the two-body scattering matrix $\mathscr{K}$ is defined by

$$\langle 12|\mathscr{K}(\omega)|34\rangle = \langle 12|K(\omega)|34\rangle \prod_{i=1,4}\sqrt{1-n(k_i)}\,, \tag{4}$$

where the scattering matrix K satisfies the integral equation

$$\langle 12|K(\omega)|34\rangle = \langle 12|V|34\rangle + \sum_{5,6}\langle 12|V|56\rangle\frac{[1-n(k_5)][1-n(k_6)]}{\omega-e_5-e_6}\langle 56|K(\omega)|34\rangle\,. \tag{5}$$

In these equations $n(k)$ is the Fermi distribution function at a given temperature and for the single-particle spectrum $e(k) = k^2/2m + U(k)$. Then Eq. (5) coincides with the Brueckner equation for the G-matrix in the zero-temperature limit. It has to be noted that only the principal part has to be considered in the integration, thus making K a real matrix. The appearance of the arctan in Eq. (5) looks peculiar, but it comes from a ladder summation similar to the one for the zero-temperature G-matrix. More details on the derivation and on the numerical treatment of the equations can be found in Ref. [26].

In this framework, the free energy is $F = \Omega + \mu A$ and the pressure is obtained from the thermodynamical relationship

$$p = \rho^2\frac{\partial(F/A)}{\partial\rho}\,, \tag{6}$$

where $\rho = A/V$ is the total number density. A typical result is reported for symmetric matter in Fig. 1, for different values of the temperature. The resulting EOS at finite temperature, i.e., pressure versus density, is shown in Fig. 2. One recognizes the familiar van der Waals shape, which entails a liquid-gas phase transition, with a definite critical temperature, i.e., the temperature at which the minimum in the van der Waals isotherm disappears. This is clearly a fundamental property of the nuclear medium: at finite temperature it behaves macroscopically in a way similar to a classical liquid. The critical temperature

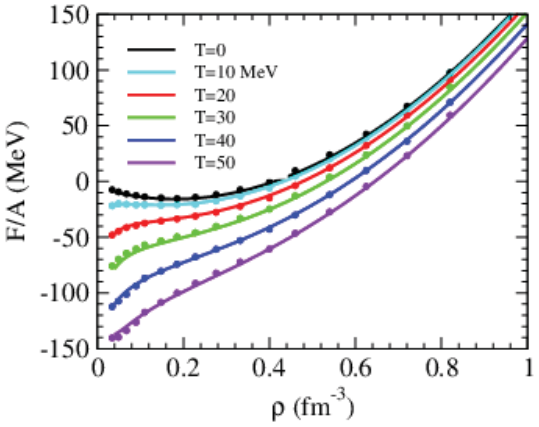

Figure 1. Free energy of symmetric nuclear matter as a function of density at different temperatures. The lines are fits to the calculated points. The curves decrease systematically as the temperature increases.

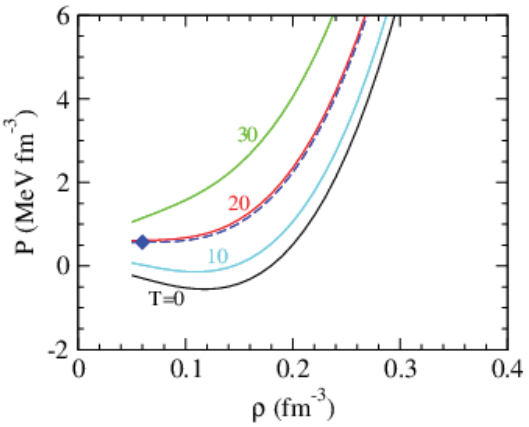

Figure 2. The pressure is displayed vs. baryon density for isotherms of symmetric nuclear matter. The full diamond marks the critical point of the liquid-gas phase transition.

turns out to be around $T_c = 18-20$ MeV. This is the result of microscopic calculations, but also of those employing effective forces, e.g., Skyrme forces. The values of the critical temperature, however, depend on the theoretical scheme, and on the particular effective force adopted.

To solve Eq. (5) one needs as input the interactions between hadrons. In the calculations presented in this paper, we have used as nucleon-nucleon two-body force the Argonne V_{18} potential [27], supplemented by three-body forces (TBF) needed in order to reproduce correctly the saturation point of nuclear matter. One should notice that both two- and three-body forces should be consistent, i.e., use the same microscopic parameters in their construction. We discuss results obtained using in the TBF the same meson-exchange parameters as the two-body potential [28]. For completeness, we also present results based on phenomenological models for TBF, such as the Urbana TBF [29], here denoted by UTBF (UIX), which consists of an attractive term due to two-pion exchange with excitation of an intermediate Δ resonance, and a repulsive phenomenological central term.

As far as the hyperonic sector is concerned, we employ the Nijmegen soft-core nucleon-hyperon (NY) potentials NSC89, which are fitted to the available experimental NY scattering data [30, 31]. Those potentials have been widely used in the BBG zero-temperature calculations [22, 23, 32, 33]. We restrict the present study to two hyperon species, Λ and Σ^-, neglecting the appearance of thermal Σ^0 and Σ^+ and heavier hyperons. Moreover we neglect hyperonic two- and three-body forces, due to the lack of experimental data.

3. Quark matter

For the deconfined quark phase, we adopt two different models, the thermodynamical MIT bag model, and one based on the Dyson-Schwinger equations of QCD.

Within the simplest form of the MIT model [34], the quarks are considered to be free inside a bag and the thermodynamic properties are derived from the Fermi distribution,

$$\tilde{f}_q(k;\tilde{\mu}_q,T) = f_q^+(k) - f_q^-(k)\,, \quad f_q^\pm(k) = \frac{1}{1+\exp[(E_q(k)\mp\tilde{\mu}_q)/T]} \tag{7}$$

with $E_q(k) = \sqrt{m_q^2+k^2}$ and $\tilde{\mu}_q$ being the auxiliary quark chemical potentials. The quark number density

is obtained from Eq. (14) and the energy density and free energy density for the quark phase are given as

$$\varepsilon_Q = B + g\sum_q \int \frac{d^3k}{(2\pi)^3}\left[f_q^+(k) + f_q^-(k)\right] E_q(k)\,, \quad f_Q = \varepsilon_Q - T\sum_q s_q^{\rm free}\,, \tag{8}$$

where B is the bag constant and $s_q^{\rm free}$ the entropy density of a noninteracting quark gas. The 'true' quark chemical potential, entropy density, and pressure are given by the general relations

$$\mu_q = \frac{\partial f_Q(\rho_u,\rho_d,\rho_s,T)}{\partial \rho_q}\,, \quad s_Q = \frac{\partial f_Q(\rho_u,\rho_d,\rho_s,T)}{\partial T}\,, \quad p_Q = \sum_q \mu_q\rho_q - f_Q\,. \tag{9}$$

We have used massless u and d quarks, and $m_s = 150$ MeV. In the following we present results based on the MIT model using both a constant value of the bag parameter, $B = 90$ MeV fm^{-3} and a Gaussian parametrization for the density dependence,

$$B(\rho) = B_\infty + (B_0 - B_\infty)\exp\left[-\beta\left(\frac{\rho}{\rho_0}\right)^2\right] \tag{10}$$

with $B_\infty = 50$ MeV fm^{-3}, $B_0 = 400$ MeV fm^{-3}, and $\beta = 0.17$, see Ref. [35]. For a more extensive discussion of this topic, the reader is referred to Refs. [35, 36].

The other quark matter model is based on the Dyson-Schwinger equations, which provide a continuum approach to QCD and can simultaneously address both confinement and dynamical chiral symmetry breaking [14, 15]. It has been applied with success to hadron physics in vacuum [37, 38, 39], and to QCD at nonzero chemical potential and temperature [40, 41]. Recently efforts have been made to calculate the EOS for cold quark matter and compact stars [42, 16], and later it has been extended to the finite-temperature case [17]. The starting point is QCD's gap equation for the quark propagator $S(\boldsymbol{p},\omega_n;\mu,T)$ at finite quark chemical potential μ, employing an in-medium gluon propagator

$$D_{\mu\nu}(\boldsymbol{k},\Omega_n) = P^T_{\mu\nu}D_T(\boldsymbol{k}^2,\Omega_n^2) + P^L_{\mu\nu}D_L(\boldsymbol{k}^2,\Omega_n^2) \tag{11}$$

with the gluon Matsubara frequency $\Omega_n = 2n\pi T$,

$$P^T_{\mu\nu} = \begin{cases} \delta_{\mu\nu} - k_\mu k_\nu/\boldsymbol{k}^2 & \mu,\nu = 1,2,3 \\ 0 & \mu,\nu = 4 \end{cases}\,, \quad P^L_{\mu\nu} = P_{\mu\nu} - P^T_{\mu\nu} \tag{12}$$

and

$$D_T(\boldsymbol{k}^2,\Omega_n) = D_L(\boldsymbol{k}^2,\Omega_n) = \frac{4\pi^2 D}{\omega^6}\mathrm{e}^{-\alpha\mu^2/\omega^2}k^2\,\mathrm{e}^{-k^2/\omega^2}\,, \tag{13}$$

with only a chemical potential dependence of the coupling strength, quantified by the parameter α, but neglecting any temperature effects. As in Ref. [16], we choose the set of parameters $\omega = 0.5$ GeV, $D = 1$ GeV^2 and use two typical values $\alpha = 2$ and $\alpha = 4$ in our calculation.

The quark propagator is the main input for calculating the single-flavor quark number density as

$$\rho_q(\mu_q,T) = g\int \frac{d^3p}{(2\pi)^3}\,\tilde{f}_q(|\boldsymbol{p}|;\mu_q,T)\,, \quad \tilde{f}_q(|\boldsymbol{p}|;\mu_q,T) = \frac{T}{2}\sum_{n=-\infty}^{\infty}\mathrm{tr_D}\left[-\gamma_4 S_q(\boldsymbol{p},\omega_n;\mu_q,T)\right]\,, \tag{14}$$

where $\omega_n = (2n+1)\pi\,T$ is the Matsubara frequency for quarks, $p = (\boldsymbol{p},\omega_n)$, $g = 2N_c = 6$ is the quark degeneracy and the trace is over spinor indices only. Due to the asymptotic freedom at large chemical potential $\mu_{\rm UV}$, which we take as $\mu_{\rm UV} = 1$ GeV, the single-flavor quark thermodynamic pressure at finite chemical potential and temperature can be obtained as

$$P_q(\mu_q,T) = P_q(\mu_{q,0},0) + \int_{\mu_{q,0}}^{\mu_{\rm UV}} d\mu'\,\rho_q(\mu',0) + \int_0^T dT'\,s_q^{\rm free}(\mu_{\rm UV},T') + \int_{\mu_{\rm UV}}^{\mu_q} d\mu'\,\rho_q(\mu',T)\,. \tag{15}$$

The total pressure for the quark phase is given by summing contributions from all flavors. For comparison with the bag model, we write the pressure of the quark phase as

$$p_Q(\mu_u,\mu_d,\mu_s,T) \equiv \sum_{q=u,d,s} \tilde{p}_q(\mu_q,T) - B_{\rm DS}\,, \tag{16}$$

with the bag constant

$$B_{\rm DS} \equiv -\sum_{q=u,d,s} p_q(\mu_{q,0},0) \tag{17}$$

and the reduced pressure $\tilde{p}_q(\mu_q,T) \equiv p_q(\mu_q,T) - p_q(\mu_{q,0},0)$ from the integrals of quark number density and entropy density. As in Ref. [16], we set $B_{\rm DS} = 90$ MeV with $\mu_{u,0} = \mu_{d,0} = 0$ and $\mu_{s,0}$ as the value of the starting point of the deconfined phase of strange quarks. Further details are given in Ref. [17].

4. Phase transition and EOS

In neutrino-trapped beta-stable nuclear matter the chemical potential of any particle $i = n,p,\Lambda,\Sigma^-,u,d,s,l$ is uniquely determined by the conserved quantities baryon number B_i, electric charge Q_i, and weak charges (lepton numbers) $L_i^{(e)}$, $L_i^{(\mu)}$ with corresponding chemical potentials $\mu_B,\mu_Q,\mu_{L_e},\mu_{L_\mu}$:

$$\mu_i = B_i\mu_B + Q_i\mu_Q + L_i^{(e)}\mu_{L_e} + L_i^{(\mu)}\mu_{L_\mu}\,, \tag{18}$$

where $B_i, Q_i, L_i^{(e)}, L_i^{(\mu)}$ are the corresponding charges of each particle. The relations of chemical potentials and densities for hadrons and quarks are given in the previous sections, and we treat leptons as free fermions. With such relations, the whole system in each phase can be solved for a given baryon density $\rho_B = \sum_i B_i\rho_i$, imposing the charge neutrality condition $\sum_i Q_i\rho_i = 0$ and lepton number conservation $Y_l\rho_B = \sum_i L_i^{(l)}\rho_i$. We fix the lepton fractions to $Y_e = 0.4$ for neutrino-trapped matter at $T = 40$ MeV, and we neglect muons and muon-neutrinos due to their low fractions, hence $Y_\mu = 0$. When the neutrinos ν_e are untrapped, the lepton number is not conserved any more, the density and the chemical potential of ν_e vanish, and the above equations simplify accordingly.

We study in the following the phase transition at finite temperature with the Gibbs construction [18, 43, 44, 45], which determines a range of baryon densities where both phases coexist, yielding an EOS containing a pure hadronic phase, a mixed phase, and a pure QM region. In the Gibbs construction [43] the stellar matter is treated as a two-component system, and therefore is parametrized by two chemical potentials. Usually the pair (μ_e,μ_n), i.e., electron and baryon chemical potential, is chosen. By imposing mechanical, chemical, and thermal equilibrium, it turns out that the pressure is a monotonically increasing function of the density, at variance with the Maxwell construction, where a plateau in the pressure vs. density plane exists. The Gibbs phase transition has been widely studied in the literature, and the formalism will not be repeated here.

The solid black curves in Fig. 3 represent the hadronic phases obtained with the Argonne V_{18} NN potential supplemented by microscopic TBF (upper panels) or phenomenological Urbana TBF (lower panels). The other curves are the results for beta-stable QM, i.e., the Dyson-Schwinger results with $\alpha = 2$ (dash-dot-dotted blue) and $\alpha = 4$ (dotted red), whereas the other two lines represent the results obtained with the MIT bag model, using either a constant bag parameter $B = 90\,\mathrm{MeV\,fm^{-3}}$ (dashed green) or a density-dependent $B(\rho)$ (dash-dotted pink). The thick lines denote the corresponding mixed phase. The left-hand panels display results for cold beta-stable matter, the central panels for hot ($T = 40$ MeV) and untrapped matter, and the right-hand panels for hot and trapped matter.

We find that the phase transition from hadronic to QM occurs at low values of the baryon density when the MIT bag model is used to describe the quark phase. This holds true irrespective of the EOS adopted for the hadronic matter, since the TBF effects are only important at high densities. On the contrary, with the DSM for QM the phase transition occurs at higher values of the density, since the EOS is generally

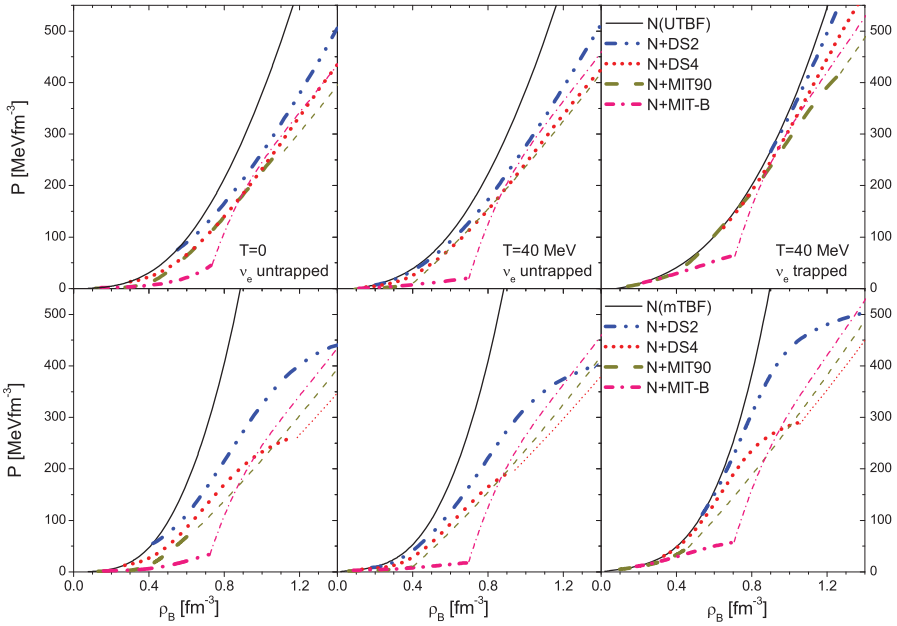

Figure 3. Pressure vs. baryon density of NS matter with the Gibbs phase transition construction for different models. Phenomenological (upper panels) or microscopic (lower panels) TBF are used for the hadronic EOS. The pure hadron or quark phases are marked with thin curves and the mixed phase region with thick curves.

stiffer than the hadronic one. In this case, the onset and the width of the density range characterizing the phase transition depend strongly on the EOS used for the hadronic phase.

Thermal effects play an important role, since they shift the onset of the phase transition to lower values of the baryon density. Neutrino trapping lowers even more the transition density in the MIT case, but increases it for the DSM. This is due to the properties of the nucleonic EOS: At low density, corresponding to the transition density in the MIT case, neutrino trapping increases the pressure and decreases the transition density. At large density, corresponding to the transition density in the DSM case, nuclear matter has a larger symmetry energy, and the decrease of nucleon pressure overwhelms the increase from the leptons. Therefore, neutrino trapping decreases the total pressure and increases the transition density. We have also found that with the DSM no phase transition exists if the hadronic phase contains hyperons and the EOS is very soft, or if the parameter α is too small and the EOS of QM is very stiff, in analogy with the zero-temperature case [16]. Taking all effects into account, the EOS comprising the phase transition turns out to be softer than the hadronic one.

The phase transitions constructed with the DSM and the MIT bag model turn out to be quite different. In the former case, the onset of the phase transition is shifted to a larger baryonic density and the mixed phase is extended to a much larger region. Different nuclear EOSs also affect the onset and the width of the mixed phase, in particular when the DS model is used. In the case of a stiff EOS for the hadronic phase with the microscopic TBF, the onset of the mixed phase is at lower density and the mixed phase has a smaller region, compared to the case of phenomenological TBF. These all have consequences for the internal structure of a PNS, as discussed now.

5. Proto-neutron star structure

The stable configurations of a (P)NS can be obtained from the well-known hydrostatic equilibrium equations of Tolman, Oppenheimer, and Volkov [1], which provide the mass-central density relation. In the low-density range, where nucleonic clustering sets in, we cannot use the BHF approach, and

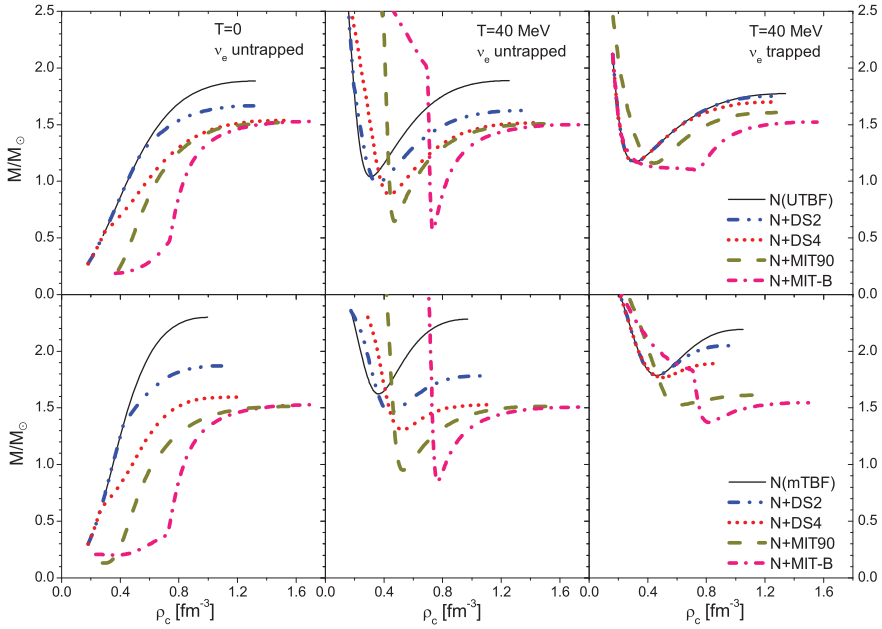

Figure 4. NS gravitational mass vs. central baryon density. Phenomenological (upper panels) or microscopic (lower panels) TBF are used for the hadronic EOS.

therefore we join [9] the BHF EOS to the finite-temperature Shen EOS [46], which is more appropriate at densities $\rho \leq 0.07$ fm^{-3}, since it does include the treatment of finite nuclei.

Our results, using the different EOSs introduced in the previous section, are displayed in Fig. 4, which shows the gravitational mass (in units of the solar mass $M_\odot = 1.98 \times 10^{33}$g) as a function of the central baryon density. We use the same conventions as in the previous figures: The black solid curves represent the calculations performed for purely hadronic matter, using either phenomenological (upper panels) or microscopic (lower panels) TBF. The colored broken curves denote stellar configurations of hybrid (P)NSs with neutrino-free (left and central panels) and neutrino-trapped matter (right panels). We notice that the value of the maximum mass decreases in neutrino-free matter due to thermal effects, both in the purely hadronic case and including the hadron-quark phase transition, where the decrease depends on the EOS used for the quark phase and turns out to be more relevant for the DS model. On the contrary, neutrino trapping decreases further the maximum mass of purely hadronic stars, but increases the value of the maximum mass of hybrid stars, overcoming the thermal effect. Therefore in this case a delayed collapse scenario is possible, just as for hyperon stars [10]. One also notices a dependence on the EOS used for the hadronic phase, which is more important for the DS model, where the QM onset takes place in a range of densities where TBF play an important stiffening role, and this explains the different values of the maximum mass. On the contrary, with the MIT bag model the transition takes place at low baryon densities where the different TBF behave similarly, hence the small influence. We find a maximum mass exceeding 2 $M_\odot$ for the hybrid configurations obtained with the microscopic TBF and suitable values of the parameter α in the DSM.

6. Conclusions

Extending the work of Ref. [16] to finite temperature, we have studied the properties of hybrid PNSs based on a hadronic BHF EOS involving different nuclear TBF joined via a Gibbs construction to the DSM quark EOS. This is only possible if hyperons are excluded from the hadronic phase.

We find a sizeable dependence of the results, in particular for the PNS maximum mass, on the nuclear TBF and on the quark model employed. The DSM model allows to reach larger masses than the MIT

model, depending on the value of the interaction strength parameter. In all cases finite temperature reduces slightly the maximum mass, but neutrino trapping increases it sufficiently for hybrid stars, such that a delayed collapse might be possible in principle.

References

[1] Shapiro S L and Teukolsky S A 1983 *Black Holes, White Dwarfs, and Neutron Stars* (New York : John Wiley & Sons)
[2] H. Bethe H 1990 *Rev. Mod. Phys.* **62** 801
[3] Burrows A and Lattimer J M 1986 *Astrophys. J.* **307** 178
[4] Prakash M, Bombaci I, Prakash M, Ellis P J, Lattimer J M and Knorren R 1997 *Phys. Rep.***280** 1
[5] Pons J A, Reddy S, Prakash M, Lattimer J M and Miralles J A 1999 *Astrophys. J.***513** 780
[6] Prakash M, Cooke J R and Lattimer J M 1995 *Phys. Rev.* D **52** 661
Steiner A W, Prakash M and Lattimer J M 2000 *Phys. Lett.* B **486** 239
Pons J A, Steiner A W, Prakash M and Lattimer J M 2001 *Phys. Rev. Lett.* **86** 5223
[7] Nicotra O E, Baldo M, Burgio G F and Schulze H-J 2006 *Astron. Astrophys.***451** 213
[8] Burgio G F and Schulze H-J 2009 *Phys. Atom. Nuc.***72** 1197
[9] Burgio G F and Schulze H-J 2010 *Astron. Astrophys.* **518** A17
[10] Burgio G F, Schulze H-J and Li A 2011 *Phys. Rev.* C **83** 025804
[11] Nicotra O E, Baldo M, Burgio G F and Schulze H-J 2006 *Phys. Rev.* D **74** 123001
[12] Yasutake N, Burgio G F and Schulze H-J 2011 *Phys. Atom. Nucl.* **74** 1502
[13] Chen H, Burgio G F, Schulze H-J and Yasutake N 2013 *Astron. Astrophys.* **551** A13
[14] Roberts C D and Williams A G 1994 *Prog. Part. Nucl. Phys.* **33** 477
[15] Alkofer R and von Smekal L 2001 *Phys. Rep.* **353** 281
[16] Chen H, Baldo M, Burgio G F and Schulze H-J 2011 *Phys. Rev.* D **84** 105023
[17] Chen H, Baldo M, Burgio G F and Schulze H-J 2012 *Phys. Rev.* D **86** 045006
[18] Glendenning N K 2000 *Compact Stars, Nuclear Physics, Particle Physics, and General Relativity* (New York : Springer).
[19] Baldo M, Bombaci I and Burgio G F 1997 *Astron. Astrophys.* **328** 274
[20] Akmal A, Pandharipande V R and Ravenhall D G 1998 *Phys. Rev.* C **58** 1804
[21] Zhou X R, Burgio G F, Lombardo U, Schulze H-J and Zuo W 2004 *Phys. Rev.* C **69** 018801
[22] Li Z H and Schulze H-J 2008 *Phys. Rev.* C **78** 028801
[23] Schulze H-J, Polls A, Ramos A and Vidaña I 2006 *Phys. Rev.* C **73** 058801
[24] Schulze H-J and Rijken T 2011 *Phys. Rev.* C **84** 035801
[25] Bloch C and De Dominicis C 1958 *Nucl. Phys.* **7** 459; Bloch C and De Dominicis C 1959 *Nucl. Phys.* **10** 181
[26] Baldo M and Ferreira L S 1999 *Phys. Rev.* C **59** 682
[27] Wiringa R B, Stoks V G J and Schiavilla R 1995 *Phys. Rev.* C **51** 38
[28] Li Z H, Lombardo U, Schulze H-J and Zuo W 2008 *Phys. Rev.* C **77** 034316
[29] Carlson J, Pandharipande V R and Wiringa R B 1983 *Nucl. Phys.* A **401** 59
[30] Maessen P M M, Rijken Th A and de Swart J J 1989 *Phys. Rev.* C **40** 2226
[31] Rijken Th A, Stoks V G J and Yamamoto Y 1999 *Phys. Rev.* C **59** 21
[32] Schulze H-J, Baldo M, Lombardo U, Cugnon J and Lejeune A 1998 *Phys. Rev.* C **57** 704
Baldo M, Burgio G F and Schulze H-J 1998 *Phys. Rev.* C **58** 3688
Baldo M, Burgio G F and Schulze H-J 2000 *Phys. Rev.* C **61** 055801
[33] Vidaña I, Polls A, Ramos A, Hjorth-Jensen M and Stoks V G J 2000 *Phys. Rev.* C **61** 025802
[34] Chodos A, Jaffe R L, Johnson K, Thorn C B and Weisskopf V F 1974 *Phys. Rev.* D **9** 3471
[35] Burgio G F, Baldo M, Sahu P K, and Schulze H-J 2002 *Phys. Rev.* C **66** 025802
[36] Maieron C, Baldo M, Burgio G F and Schulze H-J 2004 *Phys. Rev.* D **70** 043010
[37] Maris P and Roberts C D 2003 *Int. J. Mod. Phys.* E **12** 297
[38] Eichmann G, Cloet I C, Alkofer R, Krassnigg A and Roberts C D 2009 *Phys. Rev.* C **79** 012202
[39] Chang L and Roberts C D 2009 *Phys. Rev. Lett.* **103** 081601
[40] Chen H, Yuan W, Chang L, Liu Y X, Klähn T and Roberts C D 2008 *Phys. Rev.* D **78** 116015
[41] Qin S X, Chang L, Chen H, Liu Y X and Roberts C D 2011 *Phys. Rev. Lett.* **106** 172301
[42] Klähn T, Roberts C D, Chang L, Chen H and Liu Y X 2010 *Phys. Rev.* C **82** 035801
[43] Glendenning N K 1992 *Phys. Rev.* D **46** 1274
[44] Maruyama T, Chiba S, Schulze H-J and Tatsumi T 2007 *Phys. Rev.* D **76** 123015
[45] Yasutake N, Maruyama T and Tatsumi T 2009 *Phys. Rev.* D **80** 123009
[46] Shen H, Toki H, Oyamatsu K and Sumiyoshi K 1998 *Prog. Theor. Phys.* **100** 1013;
http://user.numazu-ct.ac.jp/∼sumi/eos/index.html.